



A brief overview of 8 m prototype facility of laser interferometer for Taiji pathfinder mission

Yu-Qiong Li¹ · Gang Jin¹

Received: 24 February 2020 / Accepted: 11 May 2021 / Published online: 22 May 2021
© The Author(s), under exclusive licence to Springer-Verlag GmbH Germany, part of Springer Nature 2021

Abstract

The 8 m laser interferometer prototype facility is currently being constructed at the Institute of Mechanics, Chinese Academy of Sciences in Beijing, China. It aims to perform laser interferometer experiments and pico-meter precision detection and calibration for Taiji pathfinder mission. The seismically isolated ground and passive vibration isolation are interconnected and the optical benches are stabilized by them, which can form two low-noise testbeds inside a 40 m³ ultra-high vacuum system. An on-ground laser interferometer demonstration used for satellite–satellite tracking will be constructed. In this article, the experimental facility and the employed methods will be described, and the technical details of subsystems will be covered in future papers.

1 Introduction

The laser interferometer is the most sensitive differential length change detector in the world [1–3]. Even if the amplitude of gravitational waves (GW) was remarkably small ($h = 1 \times 10^{-21}$), it was still observed by the LIGO (Laser Interferometer Gravitational-Wave Observatory) Scientific Collaboration and Virgo Collaboration using the laser interferometer method in 2016 and 2017 [4–7]. Besides the ground GW detection antennas, such as the LIGO in the United States, VIRGO in Italy [8, 9], GEO 600 in Germany [10, 11], and KAGRA in Japan [12, 13] etc., the European Space Agency (ESA) and China have scheduled to build space GW detection antennas to listen to the GW with the frequencies from 0.1 mHz to 1 Hz, including the LISA (Laser Interferometer Space Antenna) [14–16], Taiji [17–20] and Tianqin [18, 21]. The Taiji mission put forward by the Chinese Academy of Sciences (CAS) consists of a triangle of three spacecraft in orbit around the Sun [17, 18]. The road map of the Taiji mission could be summarized into three phases, and one of the most important steps is that two Taiji pathfinder satellites will be launched before 2025 [20]. The arm length is set from 10,000 km to 100,000 km, and the sensitivity will reach 100 pm/ $\sqrt{\text{Hz}}$ within the frequency

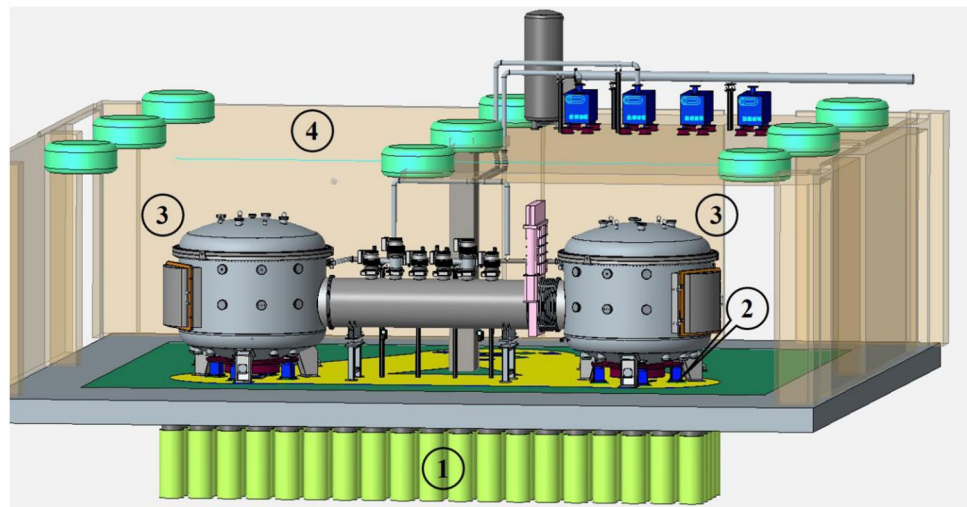
range of 0.1 mHz–1 Hz [22]. Before the Taiji pathfinder satellites being sent into the space, the laser interferometer used for satellite–satellite tracking should be simulated, demonstrated and tested in a quiet, vibration-free and ultra-high vacuum (UHV) facility for isolating the environment noises. To meet this requirement, an 8 m laser interferometer prototype facility is under construction in Beijing, China. A 40 m³ UHV system provides space environment for several simultaneous experiments. It has been designed for easy access and rapid pump down.

Based on the previous experiences [23–26], the built facility can be generally described as follows: an optical table with passive vibration isolation based on a seismically isolated ground was adopted to avoid the vibration noise, and a vacuum chamber on the seismically isolated ground was constructed to isolate the thermal and electromagnetic noises, and a clean room of 1,000 purification grade with ± 1 °C temperature adjustment precision was built to filter air and used as the primary temperature regulation system. The effect of temperature fluctuation on the laser interferometer has been investigated [23, 25, 26], and the environment noises of the laser interferometer including the vibration noise, thermal noise and electromagnetic noise can be greatly reduced by the prototype facility, of which the schematic diagram is shown in Fig. 1. Compared to the 10 m prototype interferometer facility constructed at the Albert Einstein Institute in Germany [27], the structural form of this prototype facility is similar to that, but the main applications of the two units differ greatly. The former aims to study the

✉ Yu-Qiong Li
liyqiong@imech.ac.cn

¹ National Microgravity Laboratory, Institute of Mechanics, Chinese Academy of Sciences, Beijing 100190, China

Fig. 1 Schematic diagram of the prototype facility. ① seismically isolated ground, ② passive vibration isolation, ③ vacuum chamber, ④ clean room



Standard Quantum Limit (SQL) and perform experiments for future gravitational wave detectors using advanced techniques [27]. While the major goal of this prototype facility is to design and build a satellite–satellite tracking apparatus that can be able to demonstrate and test the function of the laser interferometer. Another purpose is to detect the structure stability of core devices including the space telescope and calibrate the readout of the inertial sensor.

In this paper, each component of the prototype facility will be described. Section 2 will elaborate the seismically isolated ground and passive vibration isolation, Sect. 3 will depict the structure and performance of the vacuum system, Sect. 4 is going to describe the clean room briefly, Sect. 5 will represent the laser interferometer used for satellite–satellite tracking and some future plans, Sect. 6 will give an outlook to build a triangle of quiet, vibration-free and UHV facility based on this 8 m laser interferometer prototype facility, and Sect. 7 will summarize the work of the paper and tell the next step work in the future.

2 Seismically isolated ground and passive vibration isolation system

To simulate the triangle of three spacecraft in space, the configuration of seismically isolated ground is constructed, such as a triangle, which consists of three reinforced concrete piers and three reinforced concrete crossbeams. The diameter of the reinforced concrete pier is 3.4 m, the arm length between the centers of the two reinforced concrete piers is 8 m, and the width of each reinforced concrete crossbeam is 3 m. The height of the seismically isolated ground is 2.6 m, which consists of reinforced concrete (1.5 m, C30), concrete (0.1 m, C20) and natural mixture of sand and stone (1.0 m). The vertical view and lateral view of the seismically isolated ground are shown in Fig. 2a, b,

respectively. The weight of the seismically isolated ground is about 250 t, and the total weight of the facility above the ground is about 36 t, indicating that the weight of the seismically isolated ground is 5 times more than that of the facility, which can meet the requirement of foundation vibration reduction for payload equipment.

The vibration performance of the ground was tested by a triaxial accelerometer, which was produced by the Institute of Engineering Mechanics, China Earthquake Administration. The model was GMS-100, of which the sensitive frequency domain for velocity measurement was from 0.05 Hz to 60 Hz. The tested data were analyzed with a method called Logarithmic Amplitude Spectral Density (LASD), of which the toolbox was developed by the Max Planck Institute for Gravitational Physics [28, 29]. From the previous investigations in our group it could be known that most of the vibrations were from the Z-axis (vertical to the ground), and the stress change caused by the Z-axis vibrations was the major impact on the laser interferometer measurement among the X, Y, Z axes. Meanwhile, the results showed that the X-axis and the Y-axis had the same vibration isolation effect for this prototype facility. Therefore, here only the results of the Z-axis vibration velocity were shown in Fig. 3 to see the isolation effect contrast more clearly (if the X, Y, Z three curves were all drawn in Fig. 3, they would overlap together, resulting in a lack of clarity). The results showed that the Z-axis vibration velocities of the ground base were overlapped in the lower frequency range of 0.05 Hz and 2.8 Hz, indicating that the vibration input could not be enlarged. It could also be known that the resonant frequency of the seismically isolated ground was during the frequency regime of 2.8 Hz and 12 Hz, which meant that the vibration input would be amplified slightly. From 12 Hz to 100 Hz, the seismically isolated ground exerted the vibration isolation effect due to the energy dissipation principle.

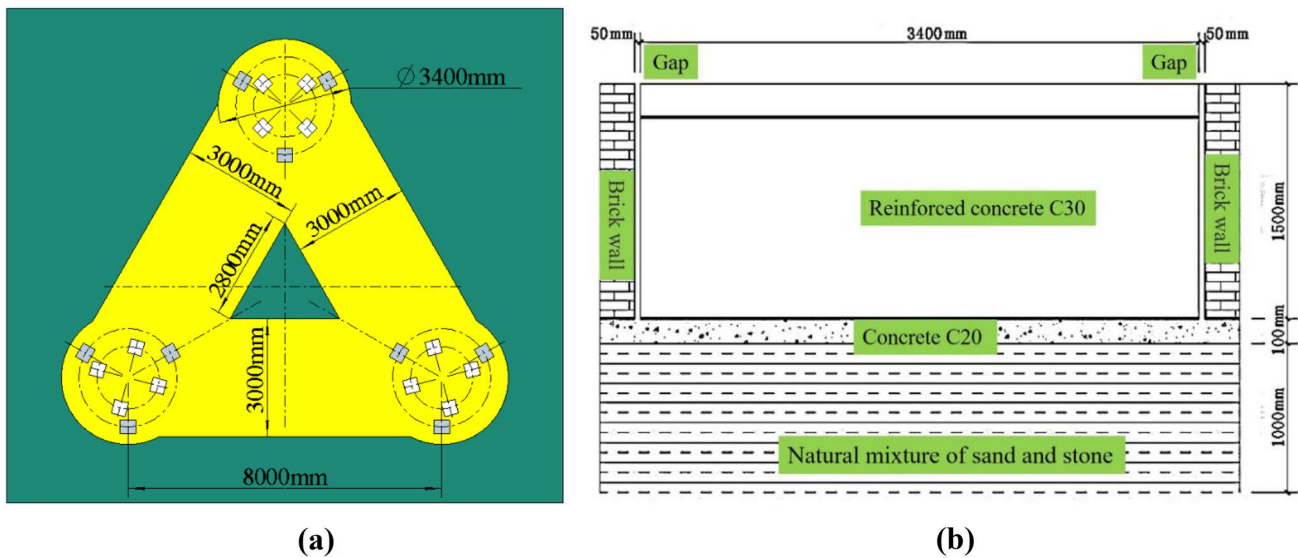
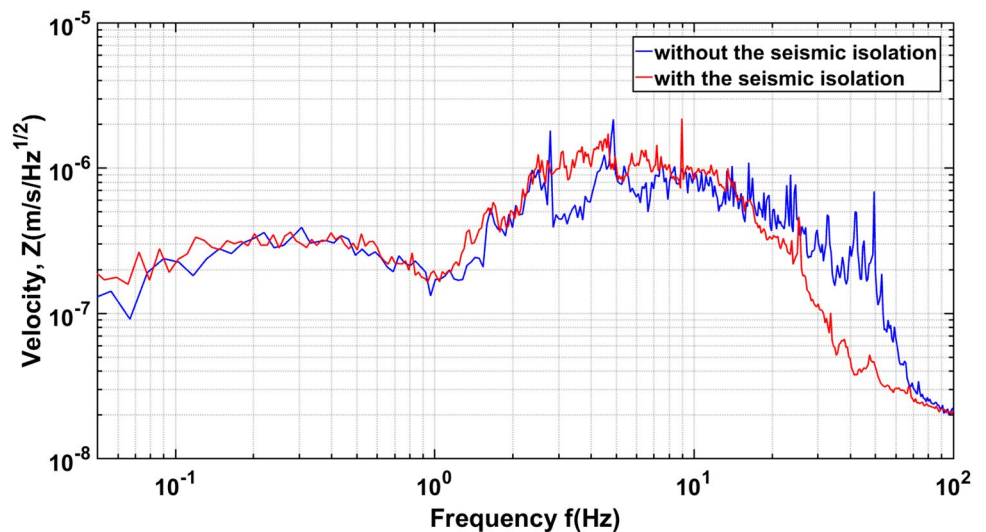


Fig. 2 Schematic diagram of the seismically isolated ground. **a** Vertical view (the yellow area is the seismically isolated ground, and the green area is the non-isolated ground), **b** lateral view

Fig. 3 Z-axis vibration velocity of the ground base



The passive vibration isolation utilizes the air floating posts (produced by the Technical Manufacturing Corporation in America, Maxdamp), which can effectively isolate the horizontal and vertical vibrations within the frequency range of 3 Hz and 100 Hz resulted from the circulating fan of the clean room and the movements of the researchers on the isolated ground. Meanwhile, from the previous investigations it can be known that the passive vibration isolation doesn't add noise in the lower frequency range of 0.1 mHz–1 Hz [26, 30]. The load-bearing of one air floating post is 1,000 kg, but here the air floating posts just support the optical platform inside the vacuum chamber, not the entire vacuum chamber. Therefore, the load-bearing of the air floating posts is enough. To maintain the stability of

the optical bench, the height of gravity center of the optical platform should be 38 cm lower than the upper surface of the posts. Therefore, it is necessary to consider the weight distribution of the optical platform. In this experimental design, it is solved by using the method of increasing the weight of the O-rings at the bottom of the optical bench legs, as shown in Fig. 4a. The diameter and thickness of the optical platform (made of stainless steel 304) are 2000 mm and 20 mm, respectively, as shown in Fig. 4b. From the size and the density (7.9 g/mm³) it can be calculated that the mass of the optical platform is about 500 kg. To prevent the optical platform from being affected by the gravity of itself or the pressure of the devices mounted on it, six reinforcement bars are added at the bottom of the optical platform. The

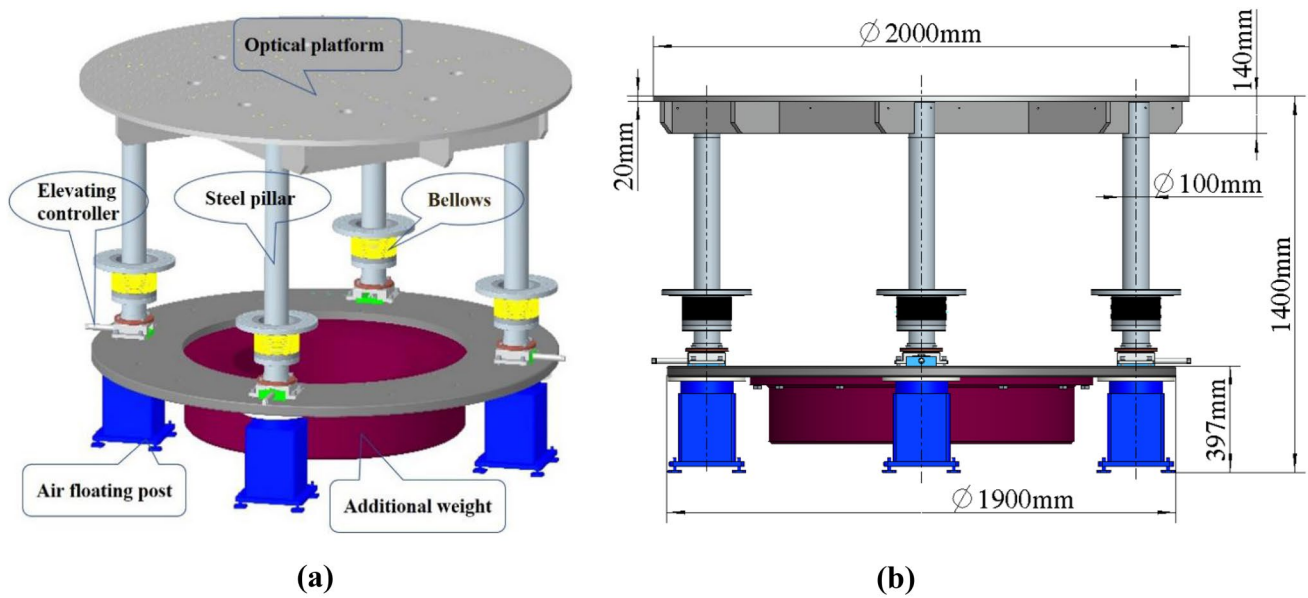


Fig. 4 Schematic diagram of the passive vibration isolation and the optical platform. **a** 3D schematic. **b** Dimensional drawing

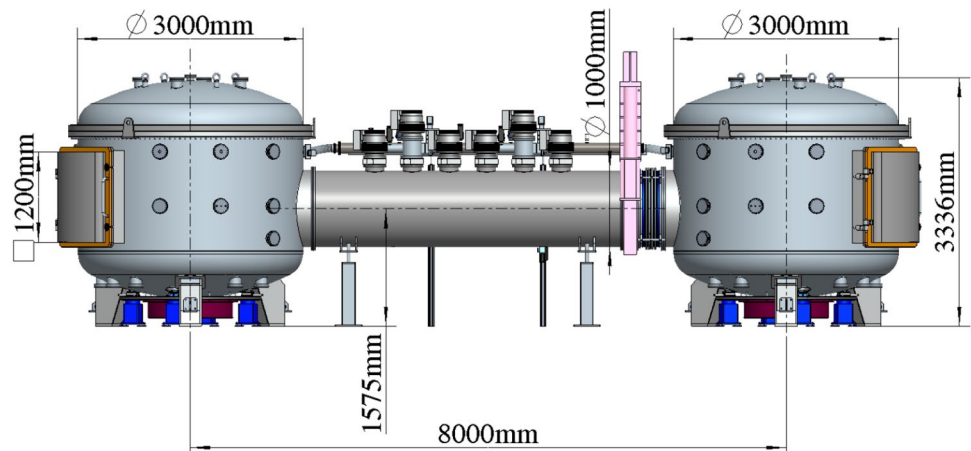
four elevating controllers are used to adjust the horizontal position of the optical platform. The bellows are adopted to separate the optical platform from the vacuum chamber, isolating the effect of the vacuum chamber vibration on the optical platform. So the vibration isolation performance of the optical platform depends on the seismically isolated ground and the passive vibration isolation.

3 Vacuum system

To reduce the thermal noise, the influence of air refractive index fluctuations and acoustic coupling, a large UHV system is adopted. Two tanks of 3.3 m height and 3 m diameter are interconnected by a 1.0 m diameter tube to form

a satellite–satellite tracking demonstration, of which the dimensional drawing is shown in Fig. 5. The center–center distance of the two tanks (the arm length) is 8.0 m, and the thickness of the chamber wall is 16 mm (stainless steel 304). To facilitate the hardware installation inside the vacuum chamber, the chamber can be entered through 1.2 m × 1.2 m doors. The large-aperture beam tubes allow light beams to be sent from any point on an optical platform to any point on the other optical platform. There is a 1.0 m diameter pneumatic slide valve to isolate the two tanks which can work independently for each other. An observation window is arranged at the top of each vacuum chamber, which is used to monitor the inside of the vacuum chamber by a camera. The vacuum feed throughs including SMA, BNC, RS232, USB and optical fiber are mounted around

Fig. 5 Dimensional drawing of the vacuum system



the vacuum chamber, which can be used to communicate and transmit information between the inside and the outside of the vacuum chamber. The electrical power feed throughs are installed at the bottom of the vacuum chamber, each chamber has 24 wires. From Fig. 4b, it can be seen that the height of the optical platform is 1400 mm, but from Fig. 5, it can be known that the center height of the 1.0 m diameter tube is 1575 mm from the ground, existing a height of 175 mm between them. The main consideration is the optical bench and laser interferometer will be setup on the optical platform, of which the height is about 175 mm.

To improve the minimum pressure of the vacuum system, the inner surface should be polished by mechanical or electrochemical polishing. However, if the surface is too smooth, the laser light will be reflected many times inside the chamber, of which the scattered light will produce a serious impact on the laser interference. To solve this contradiction, the whole inner surface is polished by the mechanical polishing firstly, then the part which the laser light can reach is ground using an emery wheel. Each component of the vacuum system must be cleaned before packaging for avoiding the optics to be polluted by the oil and dust.

Two dry screw pumps (Edwards GXS450, 450 m³/h each) pump the 40 m³ system from atmospheric pressure down to 10 Pa within 40 min, then six turbo-molecular pumps (Leybold MAG W 2200 iP DN 250 CF, 2200 l/s each) attached to the center of the tube are switched on. To improve the ultimate vacuum of the system, the operating procedures of the turbo-molecular pumps are as follows: initially, the six turbo-molecular pumps are divided into two groups, each with three turbo-molecular pumps, which is backed by one scroll pump. When the pressure reaches 1×10^{-3} Pa, a turbo-molecular pump and a dry screw pump are interconnected as the back of the other two turbo-molecular pumps in each

group, which can improve the ultimate vacuum performance of the turbo-molecular pumps. It is sufficient for most experiments that the system can pump up to 5×10^{-4} Pa within 4 h and further reach 5×10^{-5} Pa within 24 h for reducing the thermal noise and air refractive index fluctuations. Since the system cannot be baked out at high temperatures, with the limitation of partial pressure of water, its ultimate pressure can only reach 5×10^{-6} Pa. The relationship between the pressure P of the whole vacuum system and the pumping-down time t is shown in Fig. 6.

Since these pumps are running during interferometer operation, the two dry screw pumps are located in a separate room and seismically decoupled by shock-absorbing air cushions to reduce the vibration noise. While the turbo-molecular pumps are maglev, its vibration is very low (the rms value is lower than 10 nm) and decoupled by the bellows which interconnect the tube and chamber. At the same time, the optical platform and the vacuum are separated by a special isolation design, which has been elaborated in the Sect. 2. Therefore, the vibration of turbo-molecular pumps has little effect on the measurement precision of the laser interferometer. The flanges of the doors are sealed by O-rings, and the top caps are sealed by metal wires and O-rings, while other feedthroughs are sealed by copper gaskets.

To maintain the height consistency between the two optical platforms in two vacuum chamber, two methods are adopted: Firstly, embedded steel plates are planted on the surface of the seismically isolated ground as the vacuum support point, of which the height error between the two vacuum chamber is about 5 mm; Secondly, an elevating controller is planted between the passive vibration isolation and optical platform, of which the adjustable range and precision are about 2 cm and 0.1 mm, respectively. The schematic

Fig.6 Relationship between the pressure of the whole vacuum system and the pumping-down time

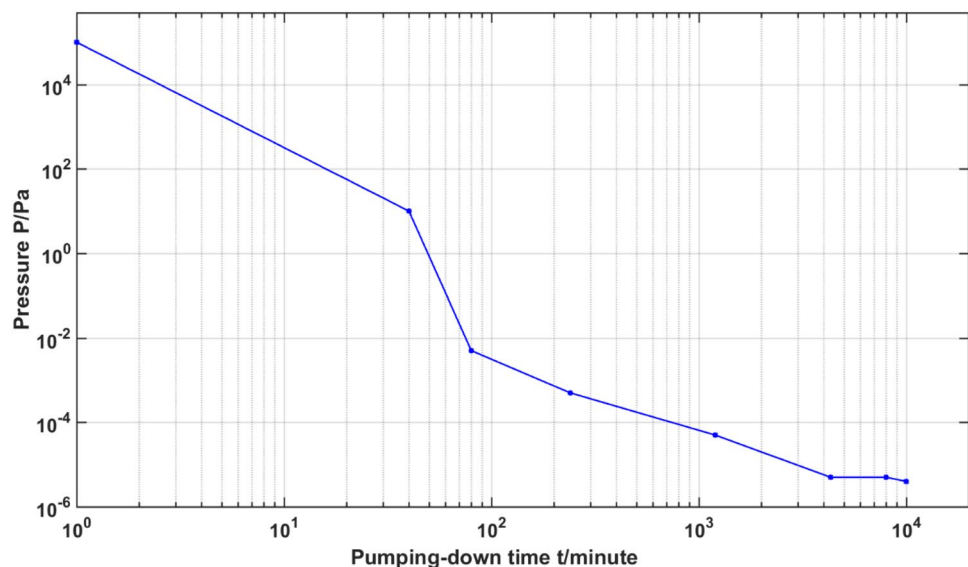


diagram of the elevating controller is shown in Fig. 7. The working principle is as follows, when the wedge structure is put forward or backward by the screw thread rotator, the steel pillar of the optical platform will be risen or fallen.

4 Clean room

To avoid the vacuum chamber and optical components to be polluted by the dust and moisture of air, a clean room with air purification, temperature and humidity regulation must be constructed, which can also act as a primary thermostat, of which the volume is 16.0 m (L) \times 16.0 m (W) \times 4.5 m (H) based on the size of the vacuum system. To reach 1,000 purification grade (measured using light scattering particle counter, around the entrance door of the vacuum chamber) with ± 1 °C temperature adjustment precision (around the vacuum chambers), the wind speed of the circulating fan must achieve 60,000 m³/h. Here the wind speed of the adopted circulating fan is 65,000 m³/h, which is produced by a Chinese corporation in Zhejiang

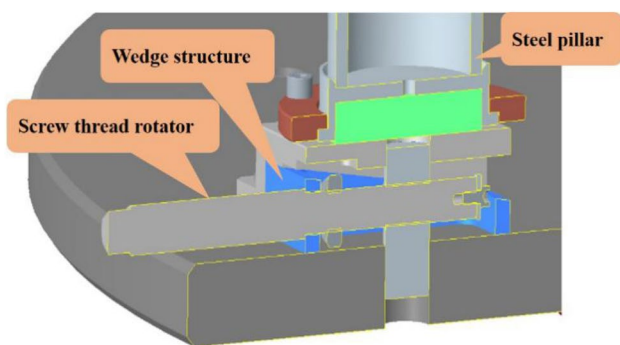
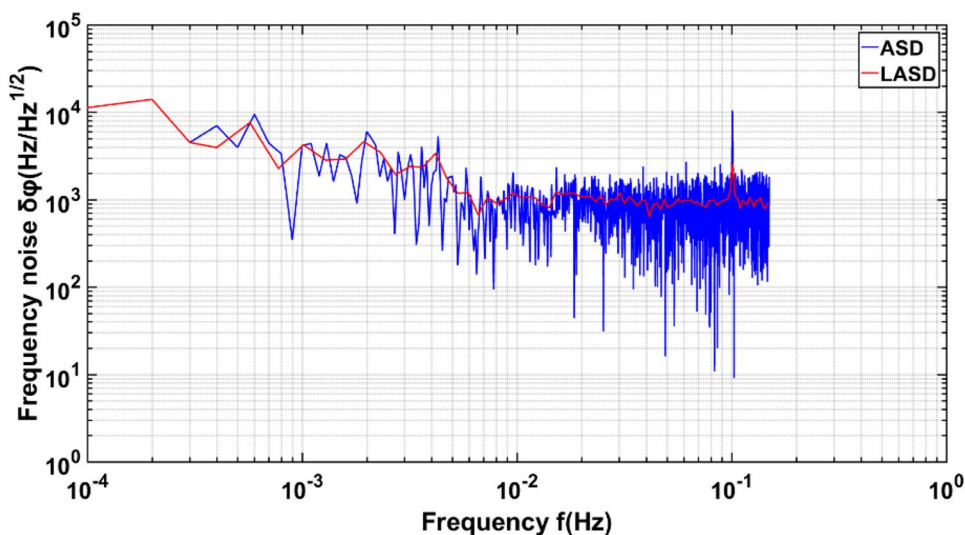


Fig. 7 Schematic diagram of the elevating controller

Fig. 8 Frequency noise of the highly stable frequency laser



province called KINGAIR. A purified-water washing room with size of 5.0 m (L) \times 5.0 m (W) \times 5.5 m (H), located at the equipment door entrance before entering the clean room, is built to clean the large-scale equipment, such as the vacuum chamber. The filtering scheme of the purification system is downflow, and the setup of the filter adopts low, medium and high three-stage filtration to effectively filter the tiny particle of the air. The humidity of the clean room can be kept from 35 to 70% when the clean filters are running. To avoid the effect of the seismic fluctuation and sound noise of the clean filters on the laser interferometer measurement, the clean filters usually are shut down when the laser interferometers are working.

5 Laser and interferometer

As the sensitivity of high precision interferometry is often limited by the frequency noise, a highly stable frequency laser is required. In this prototype facility, a highly stable frequency laser is purchased from the Stable Laser Systems in the United States. The Pound–Drever–Hall laser frequency stabilization scheme is adopted for the laser [31], of which the frequency stability is about 1 kHz/ $\sqrt{\text{Hz}}$ @ 10 mHz (as shown in Fig. 8). The output power after coupled fiber is ≥ 140 mW, and the fractional power stability is better than 0.1% / 3 h. More than 98% of the 1064 nm light is emitted in one polarized direction (the polarization extinction ratio is 22.4 dB), of which the spatial mode is TEM₀₀. The compact format laser with dimensions of 500 mm \times 600 mm footprint and 400 mm height including enclosure, of which the mass is 57 kg. The parameters of the laser are summarized in Table 1, and the physical picture is shown in Fig. 9.

The first major experiment designed for the 8 m prototype facility is an on-ground laser interferometer demonstration

Table 1 Parameters of the highly stable frequency laser

Wave-length	Power output	Frequency stability	Power stability	Spatial mode	Polarization extinction ratio
1064 nm	≥ 140 mW	1 kHz/ $\sqrt{\text{Hz}}$ @ 10 mHz	0.1%/3 h	TEM ₀₀	22.4 dB

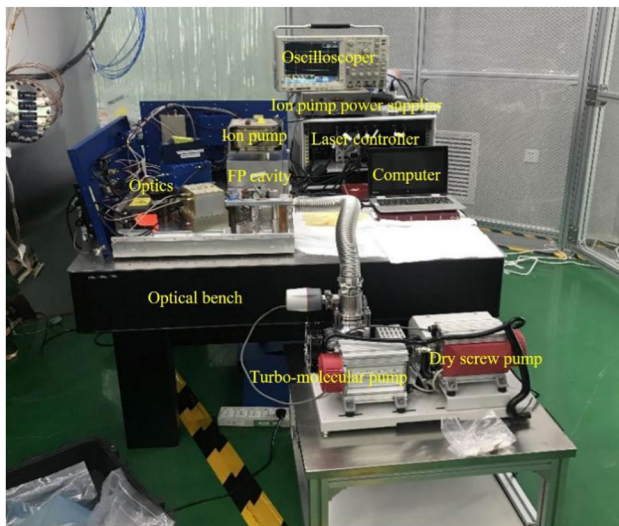


Fig.9 Physical picture of the highly stable frequency laser

used for satellite–satellite tracking, so the main consideration of laser interferometer design is a satellite–satellite tracking model. The schematic diagram of the laser interferometer is shown in Fig. 10, including two reference interferometers and two measurement interferometers, which are

shown in Fig. 11a, b, respectively. The reference interferometer senses the common-mode phase fluctuations caused by the environmental noises, such as mechanical and thermal fluctuations. It not only provides an error signal to the phase-locking of the secondary laser, but also proposes a phase reference to the other interferometers which can cancel the disturbances that don't originate on the optical bench. The measurement interferometer is sensitive to the relative distance of the two simulated testmasses to each other. Path-length fluctuations of the laser interferometers resulting from the environmental noises are measured in each individual interferometer and canceled in the differential phase 'R–M' ('R' and 'M' refer to the reference interferometer and the measurement interferometer, respectively). In the reference and measurement interferometers, laser pointing control is implemented in each interferometer to eliminate the beam pointing jitter noise, and the Differential Wave-front Sensing (DWS) technique is used to measure angular displacement [32]. Here, the primary laser is the above highly stable frequency laser, but the secondary laser is a free-running laser (Coherent, Mephisto). Therefore, a phase-locking control is formed to keep the frequency and phase of the secondary laser consistent with that of the primary laser. Many issues including arm-locking, elimination of clock jitter noise, laser ranging and data communication can also be implemented in this interferometer.

6 Outlook

The ultimate aim of the Taiji mission is schemed to send three spacecraft into space consisting of a triangle in orbit around the Sun to detect the GW signal. Therefore, the next step is to build a triangle of quite vibration-free and UHV facility based on this 8 m laser interferometer prototype

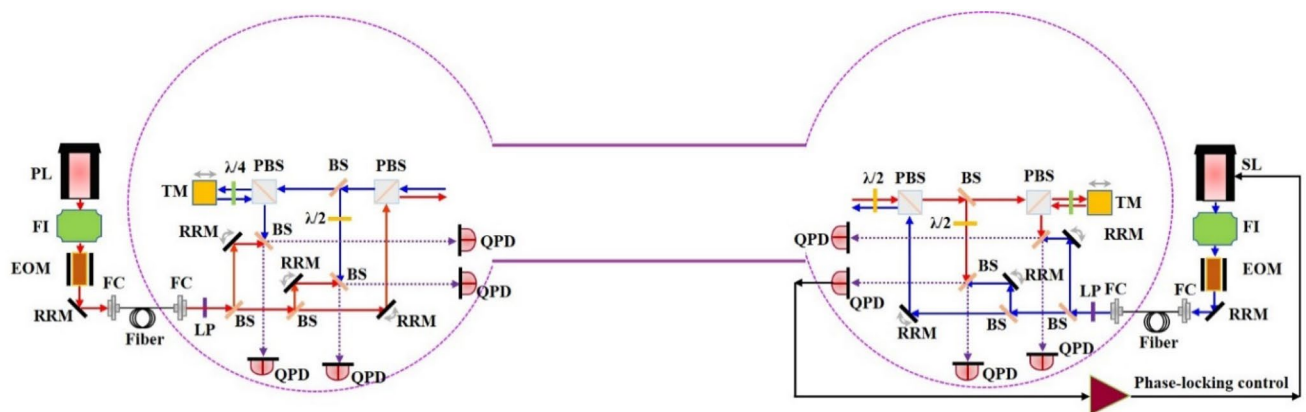


Fig.10 Schematic diagram of the laser interferometer. *PL* primary laser, *SL* secondary laser, *FI* Faraday isolator, *EOM* electro-optical modulator, *RRM* rectangular reflection mirror, *FC* fiber coupler, *LP*

linear polarizer, *BS* beam splitter, *PBS* polarizing beam splitter, *QPD* quadrant photo-detector, *TM* test-mass

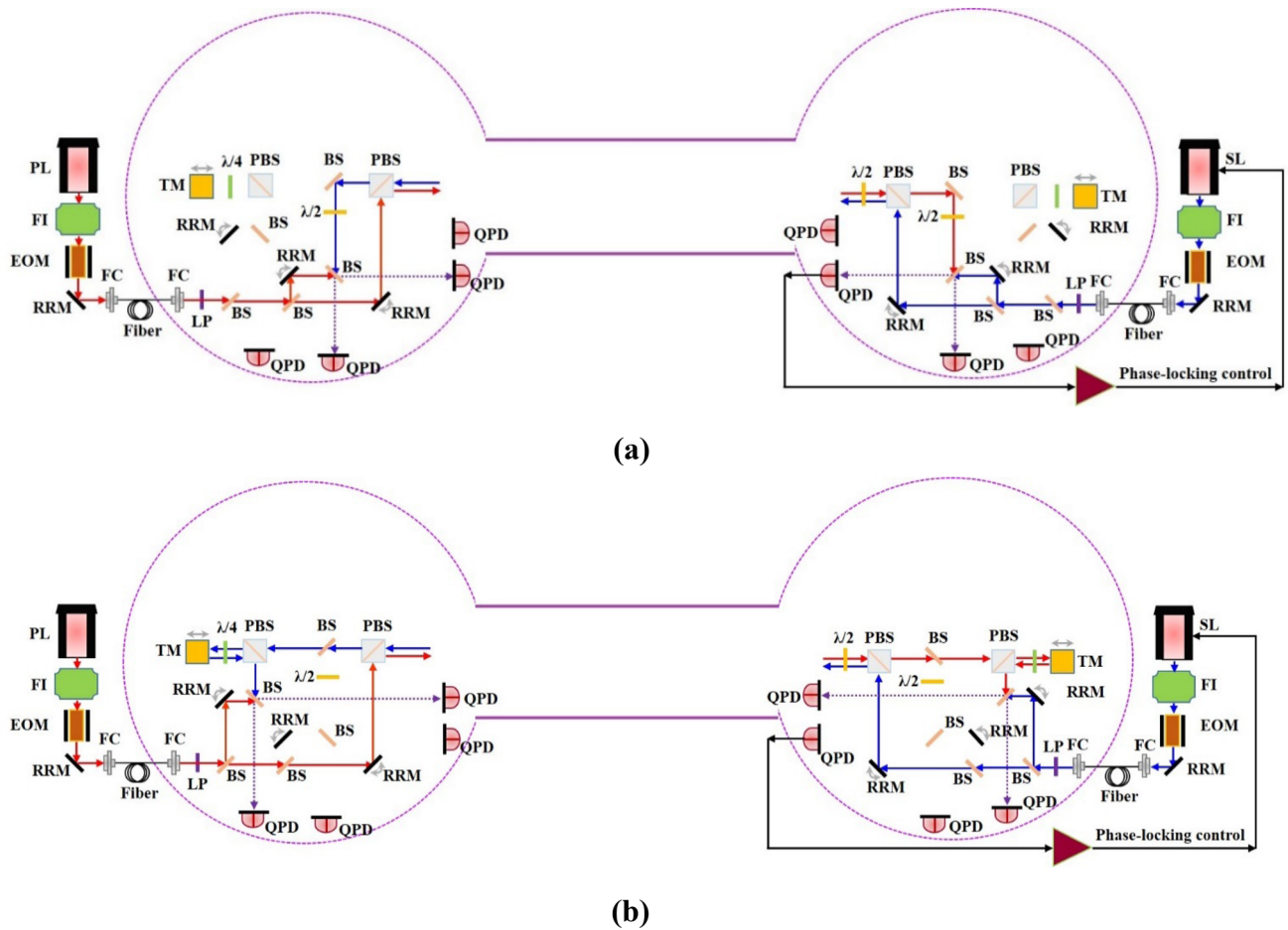


Fig. 11 Schematic diagram of the reference interferometer and measurement interferometer. **a** Reference interferometer. **b** Measurement interferometer

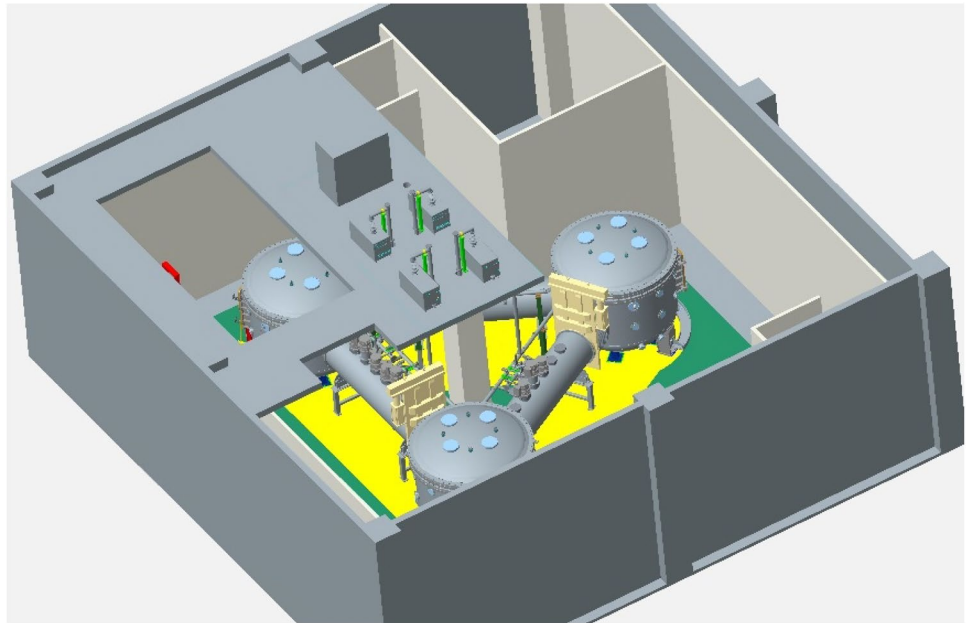
facility, which only needs to add two 1.0 m diameter tubes and one tank with a height of 3.3 m and a diameter of 3 m for other experimental facilities including seismically isolated ground and clean room have been finished. The layout of the triangle of facility is shown in Fig. 12.

7 Conclusions and future works

An 8 m laser interferometer prototype facility used for satellite–satellite tracking has been constructed, which is a key step of the development of satellite–satellite tracking laser interferometer. In this prototype facility, the seismically isolated ground exerts the vibration isolation effect due to the energy dissipation principle within

the frequency range of 12 Hz and 100 Hz, and the 40 m³ vacuum system can reach 5×10^{-4} Pa only using less than 4 h, and the clean room with dimensions of 16.0 m(L) \times 16.0 m(W) \times 4.5 m(H) achieves 1 000 purification grade with $\pm 1^\circ\text{C}$ temperature adjustment precision. Besides, a highly stable frequency laser with frequency stability of 1 kHz/ $\sqrt{\text{Hz}}$ @ 10 mHz has been assembled, and an optical path of laser interferometer integrated with phase-locking and laser pointing, etc. has also been designed. The next step is to systematically integrate all the key payloads for the space laser interferometer including the telescope, optical assembly tracking mechanism, point-ahead angle mechanism, ultra-stable clock, testmass, etc. to realize the functional demonstration and technical verification for the satellite–satellite tracking laser interferometer.

Fig. 12 Layout of the triangle of facility



Acknowledgements The authors thank the China IPPR International Engineering Co., LTD for providing the design of the seismically isolated ground, and thank the Beijing LeyFond Vacuum Tech. Co., LTD for providing the design and manufacture of the vacuum system. Besides, this work was supported by the Beijing Kechuang Platform Project, and the Strategic Priority Research Program of the Chinese Academy of Sciences (Grant No. XDB23030200), and the National Natural Science Foundation of China (Grant No. 61575209), and the Youth Innovation Promotion Association of Chinese Academy of Sciences (Grant No. 2018024), the authors express their sincere thanks for their help.

References

1. S. Nagano, T. Yoshino, H. Kunimori, M. Hosokawa, S. Kawamura, T. Sato, M. Ohkawa, *Meas. Sci. Technol.* **15**, 2406 (2004)
2. F. Acernese, M. Alshourbagy, P. Amico, F. Antonucci, S. Aoudia, K.G. Arun et al., *Class. Quantum Grav.* **25**, 184001 (2008)
3. D. Sigg (for the LIGO Scientific Collaboration), *Class. Quantum Grav.* **25**, 114041 (2008)
4. LIGO Scientific Collaboration and Virgo Collaboration, *Phys. Rev. Lett.* **116**(6), 61102 (2016)
5. LIGO Scientific Collaboration and Virgo Collaboration, *Phys. Rev. Lett.* **116**(24), 241103 (2016)
6. LIGO Scientific Collaboration and Virgo Collaboration, *Phys. Rev. Lett.* **118**(22), 221101 (2017)
7. LIGO Scientific Collaboration and Virgo Collaboration, *Phys. Rev. Lett.* **119**(14), 141101 (2017)
8. F. Acernese, F. Antonucci, S. Aoudia et al., *Astropart. Phys.* **33**(3), 182 (2010)
9. M.G. Beker, M. Bloma, J.F.J. van den Brand, H.J. Bulten, E. Hennes, D.S. Rabeling, *Phys. Procedia* **37**, 1389 (2012)
10. B. Willke, P. Aufmuth, C. Aulbert et al., *Class. Quantum Grav.* **19**(7), 1377 (2002)
11. H. Grote, *Class. Quantum Grav.*, **25**(11), 114043 (2008)
12. K. Somiya, *Class. Quantum Grav.*, **29**(12), 124007 (2011)
13. Y. Sakakibara, T. Akutsu, D. Chen et al., *Class. Quantum Grav.* **31**(22), (2014)
14. S. Rowan, J. Hough, *Living Rev. Relativ.* **14**(1), 5 (2011)
15. J.R. Gair, M. Vallisneri, S.L. Larson, J.G. Baker, *Living Rev. Relativ.* **16**(1), 1 (2013)
16. S. Vitale, *Gen. Relativ. Gravit.* **46**(5), 1730 (2014)
17. W.R. Hu, Y.L. Wu, *Natl. Sci. Rev.* **4**(5), 685 (2017)
18. D. Cyranoski, *Nature* **531**, 150 (2016)
19. X. Gong, S. Xu, S. Bai, Z. Cao, G. Chen, Y. Chen, X. He, G. Heinzel, Y.K. Lau, C. Liu, J. Luo, Z. Luo, A.P. Paton, A. Ruediger, M. Shao, R. Spurzem, Y. Wang, P. Xu, H.C. Yeh, Y. Yuan, Z. Zhou, *Class. Quantum Grav.* **28**, 094012 (2011)
20. G. Jin, *IOP Conf. Series: J. Phys.: Conf. Ser.* **840**(1), 012009 (2017)
21. J. Luo, L.S. Chen, H.Z. Duan, Y.G. Gong, S.C. Hu, J.H. Ji, Q. Liu, J.W. Mei, V. Milyukov, M. Sazhin, C.G. Shao, V.T. Toth, H.B. Tu, Y. Wang, Y. Wang, H.C. Yeh, M.S. Zhan, Y.H. Zhang, V. Zharov, Z.B. Zhou, *Class. Quantum Grav.* **33**(3), 035010 (2016)
22. H.S. Liu, Z.R. Luo, G. Jin, *Microgr. Sci. Technol.* **30**(6), 775 (2018)
23. Z.R. Luo, H.S. Liu, G. Jin, *Opt. Laser Technol.* **105**, 146 (2018)
24. Y.Q. Li, Z.R. Luo, H.S. Liu, Y.H. Dong, G. Jin, *Chin. Phys. Lett.* **29**(7), 79501 (2012)
25. Y.Q. Li, Z.R. Luo, H.S. Liu, Y.H. Dong, G. Jin, *Appl. Phys. B* **118**(2), 309 (2015)
26. Y.Q. Li, Z.R. Luo, H.S. Liu, R.H. Gao, G. Jin, *Microgr. Sci. Technol.* **30**(6), 817 (2018)
27. T. Westphal, G. Bergmann, A. Bertolini, M. Born, Y. Chen, A.V. Cumming, L. Cunningham, K. Dahl, C. Gräf, G. Hammond, G. Heinzel, S. Hild, S. Huttner, R. Jones, F. Kawazoe, S. Köhlenbeck, G. Kühn, H. Lück, K. Mossavi, J.H. Pödl, K. Somiya, A.M. van Veggel, A. Wanner, B. Willke, K.A. Strain, S. Goßler, K. Danzmann, *Appl. Phys. B* **106**, 551 (2012)
28. M. Tröbs, G. Heinzel, *Measurement* **39**, 120 (2006)
29. G. Heinzel, A. Rüdiger, R. Schilling, *Spectrum and spectral density estimation by the Discrete Fourier transform (DFT), including a comprehensive list of window functions and some new flat-top windows*. Technical Report (Albert-Einstein-Institut: Hannover, Germany 2002)

30. Y.Q. Li, C.Y. Wang, L.Y. Wang, H. Liu, G. Jin, *Microgr. Sci. Technol.* **32**, 331 (2020)
31. R.W.P. Drever, J.L. Hall, F.V. Kowalski, J. Hough, G.M. Ford, A.J. Munley, H. Ward, *Appl. Phys. B* **31**(2), 97 (1983)
32. Y.H. Dong, H.S. Liu, Z.R. Luo, Y.Q. Li, G. Jin, *Rev. Sci. Instrum.* **85**(7), 074501 (2014)

Publisher's Note Springer Nature remains neutral with regard to jurisdictional claims in published maps and institutional affiliations.